Journal of Molecular Spectroscopy 384 (2022) 111570

Contents lists available at ScienceDirect

Journal of Molecular Spectroscopy

journal homepage: www.elsevier.com/locate/yjmsp

Acetylene $\nu_1 + \nu_5$ (Π_u) ← ν_4 (Π_g) hot band revisited

N. Suas-David *, H. Linnartz, J. Bouwman[1,2,3]

Laboratory for Astrophysics, Leiden Observatory, Leiden University, PO Box 9513, 2300 RA Leiden, The Netherlands

ARTICLE INFO

Keywords:
Acetylene
Hot bands
Molecular spectroscopy
Plasma jet expansion
Cavity ring-down spectroscopy

ABSTRACT

The acetylene $\nu_1 + \nu_5$ (Π_u) ← ν_4 (Π_g) hot band has been reinvestigated at high resolution ($\leq 10^{-3}$ cm^{-1}). Vibrationally excited but rotationally cold C_2H_2 ($\approx$ 30 K) is probed in a supersonically expanding planar plasma by a continuous-wave (cw) mid-infrared cavity ring-down spectrometer at nearly Doppler free condition. Low J-value rovibrational transitions corresponding to the Q-branch are recorded for the first time. The improved resolution and newly observed transitions, combined with the existing data from the literature allow for retrieving improved molecular parameters for this hot band.

1. Introduction

Acetylene is found in a large variety of high temperature environments. On Earth, this species plays a major role in combustion chemistry, particularly in the synthesis of polycyclic aromatic hydrocarbons (PAHs) [1,2] and in the formation of soot [3]. Similar chemical mechanisms are also thought to take place in astrophysical environments such as circumstellar envelopes of AGB stars [4–8] from which dust, PAHs and other complex hydrocarbon species are expelled into the interstellar medium. Accurate spectroscopic data of acetylene associated with thermally populated vibrational levels are required to characterize the dynamics and chemical evolution of such environments.

The present work focuses on the C_2H_2 $\nu_1 + \nu_5(\Pi_u)$ ← $\nu_4(\Pi_g)$ hot band. According to recent literature reviews [9–11], only one study by Sarma et al. reported the spectral characterization of this band [12]. Their measurements were performed using an FTIR spectrometer (5.4×10^{-3} cm^{-1} apodized resolution) on acetylene contained in a gas cell and kept at 4 mbar. This room temperature experiment allowed for the identification of P- and R-branch transitions up to $J = 27$, but prohibited accurate determinations of the lower J-values, also including the Q-branch. The molecular constants that Sarma et al. used to fit the acetylene hot band were taken from a previous study by the same group [13]. In the latter paper, they fitted the spectroscopic constants of the $\nu_1 + \nu_5$ state by probing its associated cold band. The ν_4 level, not infrared active, was derived from the $(\nu_1 + \nu_4 + \nu_5 - \nu_4)^{2,0}$ ← ν_4^1 hot band and turned out to be in good agreement with an earlier study relying on the ν_5 ← ν_4 transition [14]. The only database reporting the C_2H_2 $\nu_1 + \nu_5(\Pi_u)$ ← $\nu_4(\Pi_g)$ hot band (ASD-1000 [10]) relies on an effective Hamiltonian to fit the experimental lines of the study mentioned above [12]. Some lines are extrapolated from the model as they compiled the Q-branch transitions while, to the best of our knowledge, no experimental observation has been made for this branch.

To get access to excited levels, different approaches to heat the gas (through laser excitation [15], heat exchanger [16–18]) have proved to be efficient and in this paper we are relying on the generation of a plasma in which the neutral molecules are heated by collisions with electrons in a pulsed high voltage discharge configuration [19–21]. In spectroscopy, high temperature often prevents unambiguous identifications due to the population of numerous excited states. Spectra are dense and composed of broadened lines possibly originating from blended transitions, and are consequently complex to analyze especially for highly overlapped Q-branches. The effective adiabatic cooling in supersonic free jets has been shown to be an efficient way to overcome these challenges [16,19]. In these expansions, the rotational and kinetic temperatures drop to only few tens of kelvins while the vibrational temperature remains high along the flow axis. This comes with several advantages: the lower rotational temperature increases the detection sensitivity, as the state-density increases for the lower J-levels. As higher J-levels are less populated, spectral congestion is limited.

Thus, in this manuscript we report the measured Q-branch for the C_2H_2 $\nu_1 + \nu_5(\Pi_u)$ ← $\nu_4(\Pi_g)$ hot band which is both vibrationally excited and rotationally cold, by combining plasma and supersonic expansion techniques. The higher resolution and newly recorded lines allow for retrieving improved molecular constants for this system.

2. Experimental setup

In the present experiment, a 1.3 ms long gas pulse of C_2H_2 (0.5%)/Ar is generated using a solenoid valve and admitted into the vacuum chamber

* Corresponding author.
E-mail address: suas@strw.leidenuniv.nl (N. Suas-David).
[1] Present address: Laboratory for Atmospheric and Space Physics, University of Colorado, Boulder, CO 80303 USA.
[2] Present address: Department of Chemistry, University of Colorado, Boulder, CO 80309, USA.
[3] Present address: Institute for Modeling Plasma, Atmospheres and Cosmic Dust (IMPACT), University of Colorado, Boulder, CO 80303, USA.

https://doi.org/10.1016/j.jms.2021.111570
Received 24 November 2021; Received in revised form 17 December 2021; Accepted 18 December 2021
Available online 6 January 2022

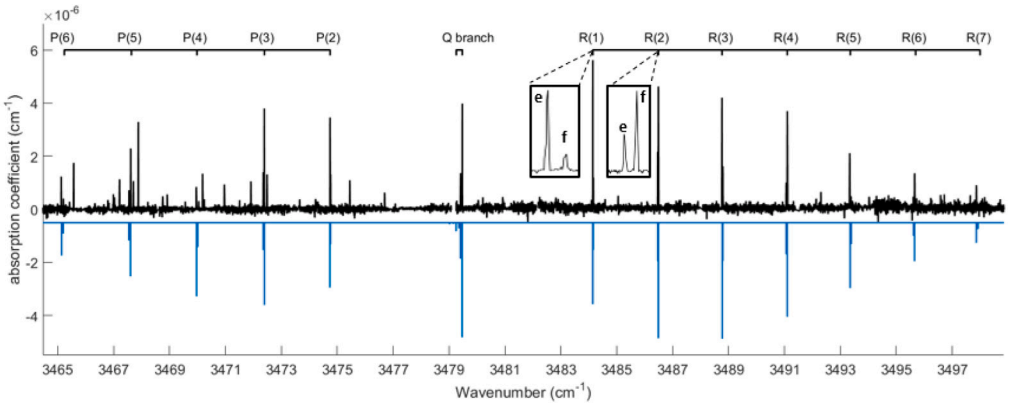

Fig. 1. The C_2H_2 $\nu_1 + \nu_5(\Pi_u) \leftarrow \nu_4(\Pi_g)$ experimental (black) and simulated (blue) spectra. The $R(1)$ and $R(2)$ l-type doublets are highlighted inside a black frame.

through a slit (500 μm × 3 cm) [22]. An abnormal glow discharge is triggered by pulsing a relatively low voltage (−300 V) over the expanding gas, slightly above the breakdown voltage. This condition is sufficient to warm the gas to a high temperature (around 1000 K) while preventing significant dissociation of acetylene which would lower the signal intensity and increase the number of transitions from byproducts. The expanding gas crosses the optical axis of a high-finesse cavity approximately 10 mm downstream and aligned parallel to the slit orifice. The 54 cm long cavity acts as resonator for a continuous-wave cavity ring-down spectrometer (cw-CRDS) with typical ring down times of the order of 8 μs. The combination of a longer effective absorption pathlength through the plasma (130 m) and highly populated low J-levels makes this detection scheme very sensitive and compensates the lower density associated with free jets. The high resolution IR spectra ($\lesssim 10^{-3}$ cm^{-1}) rely on a cw OPO laser system. The wavelength calibration in the 3465–3500 cm^{-1} region is achieved using a Bristol 621A wavemeter associated with an absolute accuracy of 5×10^{-4} cm^{-1}. The calibration procedure in the wavelength region of interest is challenging and more details are provided in the next section. Line profiles are further improved (FWHM $\approx 2\times10^{-3}$ cm^{-1}) by a reduced Doppler broadening that results from the slit geometry. The experiment runs at a repetition rate of 25 Hz and time-gates are used to only acquire the signal associated with a gas pulse. Further details are available from Refs. [22,23].

3. Calibration

The challenge in the present cw-CRDS configuration is the accurate calibration of the line positions. The free-space wavemeter used for this study is very sensitive to the angle of incidence of the laser beam. As the relatively large rotational constant of C_2H_2 spreads the lines of the hot band over dozens of wavenumbers, the OPO tuning significantly alters the alignment with respect to the wavemeter. Fortunately, water transitions, reported in the Hitran database [24], are ubiquitous in the infrared range. However, the simultaneous measurement of water vapor along with acetylene has been discarded for the following reasons. The injection of water vapor within the expansion is ineffective because of their weak intensities at low rotational temperature, furthermore keeping a low pressure of water vapor around the free jet is prevented by the required continuous N_2 flow protecting the high-reflectivity mirrors from contamination. Thus, each rovibratinal transition of the P- and R-branches has been calibrated sequentially by first recording the C_2H_2 transition in the plasma jet and subsequently, under static conditions (similar to a regular gas cell), the closest transitions from the residual water vapor in the vacuum chamber. The Q-branch is conveniently covered in the 3479.2–3479.5 cm^{-1} range by three relatively strong H_2O transitions allowing for a very accurate calibration. The intense H_2O transitions at 300 K enable working at low pressure (typically 5×10^{-2} mbar), by simply pumping down the initial room atmosphere of the vacuum chamber, thereby drastically reducing the pressure broadening.

The determination of H_2O line positions is intrinsically hindered compared to C_2H_2 transitions due to the thermal broadening (FWHM $\approx 5\times10^{-3}$ cm^{-1} and 2×10^{-3} cm^{-1} respectively). This primary reduction of accuracy is compensated by a more suitable configuration for performing the water lines measurement. The steady conditions of the H_2O gas cell experiment allow for a larger number of ring-down times averaged per wavenumber (typically 20 instead of 3) which is associated with a unique absorption coefficient. From the C_2H_2 jet measurement, on the other hand, both the gas pulse and the plasma lead to intensity fluctuations of the absorption signal. Thus, the standard deviation for the line positions is 3×10^{-4} and 4×10^{-4} cm^{-1} for C_2H_2 and H_2O respectively, while values as small as 7×10^{-5} cm^{-1} can be achieved for the strongest transitions. Therefore, the combination of the C_2H_2 and H_2O line positions uncertainties leads to an accuracy on the calibrated C_2H_2 transitions better than 7×10^{-4} cm^{-1}.

4. Results

The C_2H_2 $\nu_1 + \nu_5(\Pi_u) \leftarrow \nu_4(\Pi_g)$ experimental and simulated spectra are shown in Fig. 1. While many lines arising in the P-branch range are due to acetylene derivatives formed in the plasma expansion, the R-branch is nearly free of transitions of other species which makes the assignment straightforward. The absence of transitions linked to the $J = 0$ level, leading to a gap of around $4\tilde{B}$ ($\tilde{B}$ being the rotational constant) between the Q-branch and the lowest transitions in P- and R-branch, is characteristic for these $\Pi - \Pi$ transitions.

The relatively large uncertainty in the line amplitudes results from both the plasma instabilities and the narrow linewidth close to the resolution of the spectrometer ($\lesssim 10^{-3}$cm^{-1}) leading to typically eight wavelength points per transition. Nevertheless, the general shape of the different branches allows a determination of the rotational temperature around 30 K, in line with earlier measurements using the same plasma nozzle. The apparent temperature around 80 K extracted from the line broadening is obviously a combination of the kinetic temperature of the isentropic core ($\lesssim$ 30 K) and a geometrical Doppler effect from the limited but not fully absent transverse velocity components. Also the contribution of the warmer boundary layers, located at the interface between the isentropic core and the residual gas in the vacuum chamber, cannot be neglected even if its influence remains limited for low J-value transitions.

The rotational l-type doublets, as illustrated in Fig. 1, associated with an alternation of the e/f components' intensities (1/3) resulting from the nuclear spin wavefunctions, are clearly resolved and allow an accurate determination of the lambda doubling constant q for both levels ($\nu_1 + \nu_5$ and ν_4). The l-type doublets spacing (noted $\delta\Lambda$ here) is independent of any calibration. For this reason, this constant has been fitted separately through the following equation:

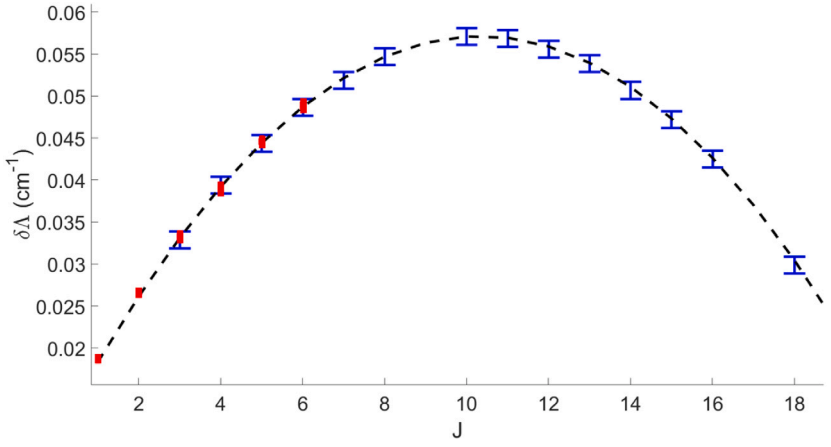

Fig. 2. Evolution of the l-doublet spacing ($\delta\Lambda$) of the R-branch as function of J. The Sarma et al. study [12] (blue) and current work (red) measurements are combined to obtain the dashed fit by refining the lambda doubling (q) constants.

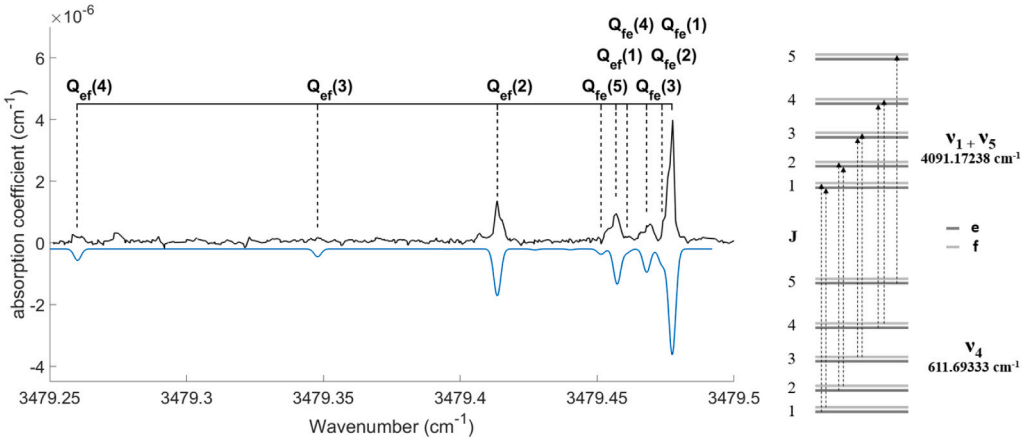

Fig. 3. Zoom in on the Q-branch presented in Fig. 1 showing the experimental (black) and simulated (blue) spectra. The diagram on the right represents the energy levels and transitions reported in this manuscript. The vibrational state origins are taken from [25].

$$\begin{aligned}\delta\Lambda(J) &= \tilde{\omega}_{ff}(J) - \tilde{\omega}_{ee}(J)\\ &= -q_{v'}J'(J'+1) - q_{Dv'}[J'(J'+1)]^2\\ &\quad + q_{v''}J''(J''+1) + q_{Dv''}[J''(J''+1)]^2\end{aligned}$$

where q and q_D are the lambda doubling and its centrifugal distortion constants of the ν_4 (v'') and $\nu_1+\nu_5$ (v') levels, while $\tilde{\omega}_{ee}$ and $\tilde{\omega}_{ff}$ are the line positions linked to the e/f components such as:

$$\tilde{\omega}_{ff/ee}(J) = E_{v'}^{f/e}(J') - E_{v''}^{f/e}(J'')$$

where the unperturbed rovibrational energy level of a linear molecule is expressed as:

$$E_v(J) = \tilde{\nu}_v + \tilde{B}_v J(J+1) - \tilde{D}_v[J(J+1)]^2 \pm \frac{1}{2}\left(q_v J(J+1) + q_{Dv}[J(J+1)]^2\right)$$

with the $\pm$ term corresponding to the e (+) and f (−) components.

The data presented here have been combined with those compiled by Sarma et al. (shown in Fig. 2 in red and blue, respectively) to recalculate the lambda doubling constants ($q_{v'}$ and $q_{v''}$) while disregarding their centrifugal distortions ($q_{Dv'}$ and $q_{Dv''}$ are taken from [12]) due to a lack of newly observed high J transitions. The fit is performed on the clear R-branch and the P-branch is used to check the accuracy of the calculation. The presence of low J-value transitions that were missing in the fit by Sarma et al. because of blended transitions (especially $R(1)$ and $R(2)$ here), along with the higher accuracy up to J=6, allows for an improvement of the lambda doubling constant determination. Despite these refinements, the overall uncertainty remains relatively high. This is also the conclusion from an independent fit of the experimental data using PGOPHER software [26] leading to the determination of the spectroscopic constants reported in Table 1. Only a further improvement in line position accuracy over a wider range of transitions will be able to address this issue.

Low J-value transitions of the Q-branch (Fig. 3) are presented here for the first time. The strong $Q_{fe}(1)$, $Q_{fe}(3)$, $Q_{ef}(1)$, $Q_{ef}(2)$, $Q_{ef}(4)$ and, to a

Table 1
Spectroscopic constants of the C_2H_2 $\nu_1+\nu_5(\Pi_u) \leftarrow \nu_4(\Pi_g)$ hot band (in cm^{-1}) determined by fitting the Q-branch from this work together with the P- and R-branches from [12]. The lambda doubling constants ($q_{v''}$ and $q_{v'}$) were determined by an independent procedure.

		Sarma et al. 1995	Current work	Shift
$G_{v'} - G_{v''}$		3479.47344 (2)	3479.47924 (4)	0.00580
ν_4	$B_{v''}$	1.1779337 (23)	1.1779376 (14)	0.0000039
	$q_{v''}(10^{-3})$	−5.23095 (52)	−5.23081 (248)	0.00014
	$D_{v''}(10^{-6})$	1.6561	1.6573 (16)	0.0012
	$q_{Dv''}(10^{-6})$	0.0399	0.0390 (30)	−0.0009
$\nu_1+\nu_5$	$B_{v'}$	1.1719945 (11)	1.1719992 (14)	0.0000047
	$q_{v'}(10^{-3})$	−4.79302 (20)	−4.79438 (251)	0.00136
	$D_{v'}(10^{-6})$	1.6432	1.6450 (16)	0.0018
	$q_{Dv'}(10^{-6})$	0.04922	0.05137 (30)	0.00215

Table 2
Comparison of the Q-branch line positions between the observed and calculated lines from the current study and the ASD-1000 database (units in cm^{-1}).

Lines	Obs.	Calc.	Obs. - Calc. (10^{-4})	ASD-1000	Calc. - ASD-1000 (10^{-4})
$Q_{fe}(1)$	3479.4773	3479.4774	−1	3479.47721	2
$Q_{fe}(2)$	–	3479.4737[a]	–	3479.47350	2
$Q_{fe}(3)$	3479.4691	3479.4682	9	3479.46792	3
$Q_{fe}(4)$	3479.4609	3479.4607	2	3479.46049	2
$Q_{ef}(1)$	3479.4568	3479.4573	−5	3479.45716	1
$Q_{fe}(5)$	–	3479.4514[b]	–	3479.45119	2
$Q_{ef}(2)$	3479.4135	3479.4136	−1	3479.41334	3
$Q_{ef}(3)$	–	3479.3478[b]	–	3479.34762	2
$Q_{ef}(4)$	3479.2600	3479.2602	−2	3479.26000	2

[a]Blended line (not used in the fit).
[b]Lines too weak to be observed (not used in the fit).

lesser extent, $Q_{fe}(4)$ lines are well resolved while the $Q_{fe}(2)$ is blended. The $Q_{fe}(5)$ and $Q_{ef}(3)$ transitions along with transitions associated with higher J-values are too weak to be observed under our experimental conditions.

Table 2 summarizes the positions of the Q-branch lines. The newly obtained values are compared to the ASD-1000 database where the line positions have been extrapolated through a global fit of the Sarma et al. data of the P-/R-branches. The difference between the ASD-1000 database and our measurement falls within our uncertainty range (7×10^{-4} cm^{-1}), except for the $Q_{fe}(3)$ which could be resulting from the partial blending of this transition. Our results show a slight shift ($\approx 2\times10^{-4}$ cm^{-1}) compared to the database but overall confirming the prediction of the line positions through the global fit.

The combination of the independent determination of the l-type doubling constants, and the new Q-branch transitions made it possible to redetermine the molecular constants, using the program PGOPHER [26]. The results are shown in Table 1 and compared to the values currently available from the literature. The standard deviation of the fit is better than 1.6×10^{-4} cm^{-1}. A good agreement with [12] is found for the υ_4 state while the lambda coupling and its centrifugal distortion constant of the $\nu_1+\nu_5$ state show significant differences. However, it should be noted that the uncertainty on the $q_{v'}$ is high. Also, the determination of the band center (3479.47924 cm^{-1}) is closer to the value presented in [25] (3479.47905 cm^{-1}) than in [12] (3479.47344cm^{-1}).

5. Conclusion

The strong out of thermal equilibrium conditions associated with a free jet expansion combined with a plasma discharge to heat the gas to high temperature offer a spectroscopic tool to investigate vibrational hot bands of molecules. The experimental determination of the Q-branch line positions and the high resolution of a very sensitive cavity ring-down spectrometer expanded and improved a previous investigation of the C_2H_2 $\nu_1+\nu_5(\Pi_u)\leftarrow\nu_4(\Pi_g)$ band. This band around 3480 cm^{-1} is both intense and separated from the high line density C-H stretch region (around 2850 to 3350 cm^{-1}) making it a potential tracer in the mid-IR for high-temperature environments associated with synthesis of complex hydrocarbons. The new data are in good agreement with the ASD-1000 database and add another level of detail to the spectroscopic constants and line positions presently available.

CRediT authorship contribution statement

N. Suas-David: Conceptualization, Methodology, Investigation, Formal analysis, Writing – original draft. **H. Linnartz:** Conceptualization, Validation, Resources, Writing – review & editing. **J. Bouwman:** Conceptualization, Validation, Funding acquisition, Writing – review & editing.

Declaration of competing interest

The authors declare that they have no known competing financial interests or personal relationships that could have appeared to influence the work reported in this paper.

Acknowledgments

JB acknowledges the Netherlands Organization for Scientific Research (Nederlandse Organisatie voor Wetenschappelijk Onderzoek, NWO) for a Vidi grant (Grant No. 723.016.006) which was used to support this work.

References

[1] C.S. McEnally, L.D. Pfefferle, B. Atakan, K. Kohse-Höinghaus, Studies of aromatic hydrocarbon formation mechanisms in flames: Progress towards closing the fuel gap, Prog. Energy Combust. Sci. 32 (3) (2006) 247–294, http://dx.doi.org/10.1016/j.pecs.2005.11.003, URL: https://www.sciencedirect.com/science/article/pii/S0360128505000602.
[2] A.M. Mebel, A. Landera, R.I. Kaiser, Formation mechanisms of naphthalene and indene: From the interstellar medium to combustion flames, J. Phys. Chem. A 121 (5) (2017) 901–926, http://dx.doi.org/10.1021/acs.jcpa.6b09735, pMID: 28072538.
[3] M. Frenklach, Reaction mechanism of soot formation in flames, Phys. Chem. Chem. Phys. 4 (2002) 2028–2037, http://dx.doi.org/10.1039/B110045A.
[4] M. Frenklach, E.D. Feigelson, Formation of polycyclic aromatic hydrocarbons in circumstellar envelopes, Astrophys. J. 341 (1989) 372–384.
[5] H. Dhanoa, J.M.C. Rawlings, Is acetylene essential for carbon dust formation? Mon. Not. R. Astron. Soc. 440 (2) (2014) 1786–1793, http://dx.doi.org/10.1093/mnras/stu401, arXiv:https://academic.oup.com/mnras/article-pdf/440/2/1786/18502661/stu401.pdf.
[6] D.S.N. Parker, R.I. Kaiser, T.P. Troy, M. Ahmed, Hydrogen abstraction/acetylene addition revealed, Angew. Chem., Int. Ed. Engl. 53 (30) (2014) 7740–7744, http://dx.doi.org/10.1002/anie.201404537.
[7] L. Zhao, R.I. Kaiser, M. Ahmed, D. Joshi, G. Veber, F.R. Fischer, A.M. Mebel, Pyrene synthesis in circumstellar envelopes and its role in the formation of 2D nanostructures, Nature Astron. 2 (2018) 413–419.
[8] G. Santoro, L. Martínez, K. Lauwaet, M. Accolla, G. Tajuelo-Castilla, P. Merino, J.M. Sobrado, R.J. Peláez, V.J. Herrero, I. Tanarro, A. Mayoral, M. Agúndez, H. Sabbah, C. Joblin, J. Cernicharo, J.A. Martín-Gago, The Chemistry of Cosmic Dust Analogs from C, C_2, and C_2H_2 in C-rich Circumstellar Envelopes, 895 (2) (2020) 97, https://doi.org/10.3847/1538-4357/ab9086.
[9] B. Amyay, A. Fayt, M. Herman, J. Vander Auwera, Vibration–rotation spectroscopic database on acetylene, $\tilde{X}^1\Sigma_g^+(^{12}C_2H_2)$, J. Phys. Chem. Ref. Data 45 (2) (2016) 023103, http://dx.doi.org/10.1063/1.4947297.
[10] O.M. Lyulin, V.I. Perevalov, ASD-1000: High-resolution, high-temperature acetylene spectroscopic databank, J. Quant. Spectrosc. Radiat. Transfer 201 (2017) 94–103, http://dx.doi.org/10.1016/j.jqsrt.2017.06.032, URL: https://www.sciencedirect.com/science/article/pii/S0022407317303655.
[11] K.L. Chubb, M. Joseph, J. Franklin, N. Choudhury, T. Furtenbacher, A.G. Császár, G. Gaspard, P. Oguoko, A. Kelly, S.N. Yurchenko, J. Tennyson, C. Sousa-Silva, MARVEL analysis of the measured high-resolution rovibrational spectra of C_2H_2, J. Quant. Spectrosc. Radiat. Transfer 204 (2018) 42–55, http://dx.doi.org/10.1016/j.jqsrt.2017.08.018, URL: https://www.sciencedirect.com/science/article/pii/S0022407317305745.
[12] Y.A. Sarma, R. D'Cunha, G. Guelachvili, R. Farrenq, V.M. Devi, D.C. Benner, K.N. Rao, Stretch-bend levels of acetylene - Analysis of the hot bands in the 3300 cm^{-1} region, J. Mol. Spectrosc. 173 (2) (1995) 574–584, http://dx.doi.org/10.1006/jmsp.1995.1258.
[13] R. D'Cunha, Y. Sarma, G. Guelachvili, R. Farrenq, Q. Kou, V. Devi, D. Benner, K. Rao, Analysis of the high-resolution spectrum of acetylene in the 2.4 μm region, J. Mol. Spectrosc. 148 (1) (1991) 213–225, http://dx.doi.org/10.1016/0022-2852(91)90048-F.
[14] V. Horneman, S. Alanko, J. Hietanen, Difference band $\nu_5-\nu_4$ of acetylene C_2H_2, J. Mol. Spectrosc. 135 (1) (1989) 191–193, http://dx.doi.org/10.1016/0022-2852(89)90365-2.
[15] J. Oomens, J. Reuss, Hot band spectroscopy of acetylene after intermolecular vibrational energy transfer from ethylene, J. Mol. Spectrosc. 173 (1) (1995) 14–24, http://dx.doi.org/10.1006/jmsp.1995.1213, URL: https://www.sciencedirect.com/science/article/pii/S0022285285712131.
[16] E. Dudàs, N. Suas-David, S. Brahmachary, V. Kulkarni, A. Benidar, S. Kassi, C. Charles, R. Georges, High-temperature hypersonic Laval nozzle for non-LTE cavity ringdown spectroscopy, J. Chem. Phys. 152 (13) (2020) 134201, http://dx.doi.org/10.1063/5.0003886.

[17] M.D. Harmony, K.A. Beran, D.M. Angst, K.L. Ratzlaff, A compact hot-nozzle Fourier-transform microwave spectrometer, Rev. Sci. Instrum. 66 (11) (1995) 5196–5202, http://dx.doi.org/10.1063/1.1146150.

[18] D.K. Bronnikov, D.V. Kalinin, V.D. Rusanov, Y.G. Filimonov, Y.G. Selianov, J.C. Hilico, Spectroscopy and non-equilibrium distribution of vibrationally excited methane in a supersonic jet, J. Quant. Spectrosc. Radiat. Transfer 60 (6) (1998) 1053–1068, http://dx.doi.org/10.1016/S0022-4073(97)00210-0, URL: https://www.sciencedirect.com/science/article/pii/S0022407397002100.

[19] D. Zhao, K.D. Doney, H. Linnartz, High-resolution infrared spectra of vibrationally excited HC_4H in a supersonic hydrocarbon plasma jet, J. Mol. Spectrosc. 296 (2014) 1–8, http://dx.doi.org/10.1016/j.jms.2013.11.008, URL: https://www.sciencedirect.com/science/article/pii/S0022285213001732.

[20] G. Bazalgette Courrèges-Lacoste, J.P. Sprengers, J. Bulthuis, S. Stolte, T. Motylewski, H. Linnartz, Vibrationally excited state spectroscopy of radicals in a supersonic plasma, Chem. Phys. Lett. 335 (3) (2001) 209–214, http://dx.doi.org/10.1016/S0009-2614(01)00017-3, URL: https://www.sciencedirect.com/science/article/pii/S0009261401000173.

[21] M.E. Sanz, M.C. McCarthy, P. Thaddeus, Vibrational excitation and relaxation of five polyatomic molecules in an electrical discharge, J. Chem. Phys. 122 (19) (2005) 194319, http://dx.doi.org/10.1063/1.1869988.

[22] T. Motylewski, H. Linnartz, Cavity ring down spectroscopy on radicals in a supersonic slit nozzle discharge, Rev. Sci. Instrum. 70 (2) (1999) 1305–1312, http://dx.doi.org/10.1063/1.1149589.

[23] D. Zhao, J. Guss, A.J. Walsh, H. Linnartz, Mid-infrared continuous wave cavity ring-down spectroscopy of a pulsed hydrocarbon plasma, Chem. Phys. Lett. 565 (2013) 132–137, http://dx.doi.org/10.1016/j.cplett.2013.02.025, URL: https://www.sciencedirect.com/science/article/pii/S0009261413002340.

[24] I.E. Gordon, L.S. Rothman, R.J. Hargreaves, R. Hashemi, E.V. Karlovets, F.M. Skinner, E.K. Conway, C. Hill, R.V. Kochanov, Y. Tan, P. Wcisło, A.A. Finenko, K. Nelson, P.F. Bernath, M. Birk, V. Boudon, A. Campargue, K.V. Chance, A. Coustenis, B.J. Drouin, J.-M. Flaud, R.R. Gamache, J.T. Hodges, D. Jacquemart, E.J. Mlawer, A.V. Nikitin, V.I. Perevalov, M. Rotger, J. Tennyson, G.C. Toon, H. Tran, V.G. Tyuterev, E.M. Adkins, A. Baker, A. Barbe, E. Cané, A.G. Császár, A. Dudaryonok, O. Egorov, A.J. Fleisher, H. Fleurbaey, A. Foltynowicz, T. Furtenbacher, J.J. Harrison, J.-M. Hartmann, V.-M. Horneman, X. Huang, T. Karman, J. Karns, S. Kassi, I. Kleiner, V. Kofman, F. Kwabia-Tchana, N.N. Lavrentieva, T.J. Lee, D.A. Long, A.A. Lukashevskaya, O.M. Lyulin, V.Y. Makhnev, W. Matt, S.T. Massie, M. Melosso, S.N. Mikhailenko, D. Mondelain, H.S.P. Müller, O.V. Naumenko, A. Perrin, O.L. Polyansky, E. Raddaoui, P.L. Raston, Z.D. Reed, M. Rey, C. Richard, R. Tóbiás, I. Sadiek, D.W. Schwenke, E. Starikova, K. Sung, F. Tamassia, S.A. Tashkun, J.V. Auwera, I.A. Vasilenko, A.A. Vigasin, G.L. Villanueva, B. Vispoel, G. Wagner, A. Yachmenev, S.N. Yurchenko, The HITRAN2020 molecular spectroscopic database, J. Quant. Spectrosc. Radiat. Transfer (2021) 107949, http://dx.doi.org/10.1016/j.jqsrt.2021.107949, URL: https://www.sciencedirect.com/science/article/pii/S0022407321004416.

[25] W.J. Lafferty, A.S. Pine, Spectroscopic constants for the 2.5 and 3.0 μm bands of acetylene, J. Mol. Spectrosc. 141 (2) (1990) 223–230, http://dx.doi.org/10.1016/0022-2852(90)90159-N, URL: https://www.sciencedirect.com/science/article/pii/002228529090159N.

[26] C.M. Western, PGOPHER: A program for simulating rotational, vibrational and electronic spectra, J. Quant. Spectrosc. Radiat. Transfer 186 (2017) 221–242, http://dx.doi.org/10.1016/j.jqsrt.2016.04.010, URL: https://www.sciencedirect.com/science/article/pii/S0022407316300437, Satellite Remote Sensing and Spectroscopy: Joint ACE-Odin Meeting, October 2015.